Cardiac Electrophysiological Activation Pattern Estimation from Images using a Patient-Specific Database of Synthetic Image Sequences

Adityo Prakosa, Maxime Sermesant, Pascal Allain, Nicolas Villain, Christopher Aldo Rinaldi, Kawal Rhode, Reza Razavi, Hervé Delingette, Nicholas Ayache

Cardiac Electrophysiological Activation Pattern Estimation from Images using a Patient-Specific Database of Synthetic Image Sequences

Adityo Prakosa, Maxime Sermesant, Pascal Allain, Nicolas Villain, C. Aldo Rinaldi, Kawal Rhode, Reza Razavi, Hervé Delingette, and Nicholas Ayache

***Abstract*—While abnormal patterns of cardiac electrophysiological activation are at the origin of important cardiovascular diseases (e.g. arrhythmia, asynchrony), the only clinically available method to observe detailed left ventricular endocardial surface activation pattern is through invasive catheter mapping. However this electrophysiological activation controls the onset of the mechanical contraction, therefore important information about the electrophysiology could be deduced from the detailed observation of the resulting motion patterns. In this article, we present the study of this inverse cardiac electro-kinematic relationship. The objective is to predict the activation pattern knowing the cardiac motion from the analysis of cardiac image sequences. To achieve this, we propose to create a rich patient-specific database of synthetic time series of cardiac images using simulations of a personalized cardiac electromechanical model, in order to study this complex relationship between electrical activity and kinematic patterns in the context of this specific patient. We use this database to train a machine learning algorithm which estimates the depolarization times of each cardiac segment from global and regional kinematic descriptors based on displacements or strains and their derivatives. Finally, we use this learning to estimate the patient's electrical activation times using the acquired clinical images. Experiments on the inverse electro-kinematic learning are demonstrated on synthetic sequences and are evaluated on clinical data with promising results. The error calculated between our prediction and the invasive intracardiac mapping ground truth is relatively small (around 10 ms for ischemic patients and 20 ms for non-ischemic patient). This approach suggests the possibility of non-invasive electrophysiological pattern estimation using cardiac motion imaging.**

I. Introduction

SINCE electrophysiological activation controls the onset of the mechanical contraction, important information about the electrophysiology could be gathered from the detailed observation of the resulting motion patterns. Abnormal patterns of this activation are at the origin of important cardiovascular diseases (e.g. arrhythmia, asynchrony). However, only catheter-based intracardiac electrical mappings are available to obtain such information, and these invasive procedures are not classically used for diagnosis but rather for planning and guiding a therapy. Electrocardiographic imaging [1] (*a.k.a.* body surface potential mapping) is a non-invasive technique for imaging activation times of the myocardium but still remains to be validated thoroughly and is not widely available in clinical centers. First application of ECGI in human subject was done in [2] to image the activation pattern of normal heart, heart with right bundle branch block, heart with pacing and also atrial flutter. In a recent study [3], the invasive catheter-based electrophysiology study findings were compared with the non-invasive ECGI method to image a large diversity of human ventricular tachycardia activation patterns. Recent validation studies were done in rabbit [4], canine [5] and swine [6] for another technique which also uses the body potential mapping, namely the three-dimensional cardiac electrical imaging (3DCEI), to non-invasively reconstruct the three-dimensional ventricular activation sequence. Another method which also used the body surface potential maps and an ultra-fast computerized tomography scanning was developed in the 3-D electrocardiographic imaging technique (3-DEIT) [7] and was compared with the 3-D intracardiac mapping in rabbits. In [8], the feasibility of the non-invasive imaging of cardiac electrophysiology (NICE) in patients with the Wolff-Parkinson-White syndrome was investigated. The result was compared with the standard invasive electroanatomic mapping. Therefore there is a strong need to quantitatively assess a patient electrophysiological condition from non-invasive imaging modalities. The proposed method could help in constraining the notoriously ill-posed inverse problem of electrocardiography.

Despite advances in both medical image analysis and intracardiac electrophysiological mapping technology, the understanding of the relationship between the cardiac electrophysiology and the cardiac motion visible in images is only partial. Since non-invasive cardiac imaging is readily available, unlike non-invasive detailed electrophysiology maps, it is important to investigate how the cardiac electrophysiology function can be estimated from the analysis of cardiac motion. This is specifically relevant, for example, in the evaluation of the Cardiac Resynchronization Therapy (CRT) where the placement and tuning of pacemaker leads play a crucial role in the outcome of the therapy. In this context, cardiologists need to interpret time series of cardiac images in order to detect and characterize kinematic patterns (motion asynchrony, delayed contraction) and then infer possible electrical conduction

A. Prakosa, M. Sermesant, H. Delingette and N. Ayache are with the Asclepios Research Project, Inria Sophia Antipolis, 2004 route des Lucioles - BP 93, 06902, Sophia Antipolis, France

P. Allain and N. Villain are with the Medisys Research Lab, Philips Healthcare France, 33 rue de Verdun - BP313, Suresnes, France

C. A. Rinaldi is with the Department of Cardiology, St. Thomas' Hospital, London, UK

K. Rhode and R. Razavi are with the King's College London, Division of Imaging Sciences, St. Thomas' Hospital, London, UK

disorders. However, currently 30% of the patients with CRT show no benefit from this therapy [9], which may be caused by the suboptimal implementation of the therapy. Providing activation maps from a time series of cardiac images would be of great interest to better select patients and to optimize the lead placements and delays during and after therapy. For instance, in a recent study, Sohal et al. [10] use time-volume curves of left ventricular segments to identify two classes of contraction patterns, which seem to be correlated with CRT response in patients with left bundle branch block (LBBB). More fundamentally, understanding the relationship between cardiac motion and electrophysiology is essential to improve the diagnosis and therapy of patients suffering from heart failure.

While there is an important literature on the estimation of the cardiac kinematics from cardiac sequences (see for instance [11], [12], [13], [14] and references therein), there exists no such tools to estimate the electrical wave propagation from such image sequences. However, the relationship between cardiac motion and electrical activation has been investigated in several studies [15], [16], [17], [18], [19].

Electromechanical Wave Imaging (EWI) modality has been recently introduced to image the Electromechanical Wave (EW) which was shown to correlate with the myocardium electrical wave propagation [18], [20]. In [21], it was shown that the EW was able to be reproduced by an E/M model. This imaging modality uses high ultrasound frequency to map the small, transient deformation of the EW. However, this method is limited to this specific modality, which has only been demonstrated in 2D (whereas the propagation pattern is 3D) and is not often available clinically.

In this paper, we propose to study the inverse electro-kinematic relationship through the creation of a patient-specific database of synthetic time series of cardiac images based on our previous study in [15]. Because it is difficult to obtain a large number of cases where both electrophysiological mapping and time series of 3D images are available, we use an E/M model of the heart to produce synthetic but visually realistic image sequences for which the electrical stimulation is known using our method [22]. On this database, invariant kinematic descriptors were extracted from each synthetic sequence and then fed to a machine learning algorithm which estimates the electrical pattern from kinematic descriptors during the cardiac cycle. The creation of this database allows us to develop this machine learning based study. Recently, many medical image analysis studies are motivated by machine learning, for example in [23] where a virtual population is created to train an active shape models. As the electro-kinematic relationship is very complex, we prefer here to generate a patient-specific database, so that the learning is done on cases relatively close to the patient condition. The hypothesis of this study is that the clinician already has some knowledge on the pathology when asking for the MR images, e.g. LBBB from a standard ECG using QRS shape and width. Therfore the aim is not to help for diagnosis but for therapy planning. We believe that solving the general case without any information on the diagnosis of the patient would lead to a huge number of possibilities and make the inverse problem even more difficult.

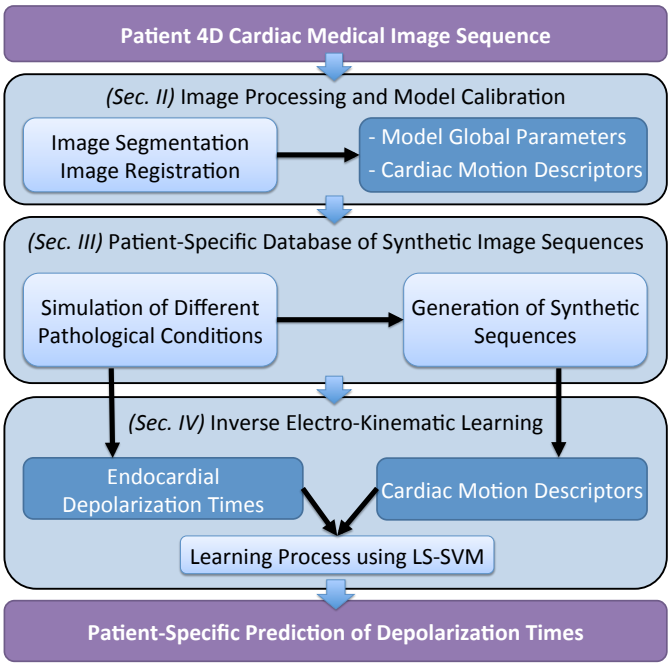

Fig. 1. **Estimation of Electrophysiological Activation Pattern from Images.** A cardiac mesh is created from image segmentation. Different electromechanical conditions are simulated close to the patient condition to generate the database of electrophysiological patterns and synthetic cardiac sequences.The relationship between the motion descriptors and the activation patterns is learned from this database. The result is used to predict the patient electrophysiological activation pattern.

Previous works [18], [19] have mainly focused in detecting E/M wave directly from the displacement and strain patterns estimated from image sequences during the contraction and relaxation of the myocardium. Since the relationship between those mechanical waves and electrical waves is very complex, our approach is to learn it through an E/M model of the heart at a larger spatial and temporal scale. In [19] the cardiac motion descriptors are combined in order to obtain the electrical activation time, but the weights are assigned manually for the descriptors. Another study by McVeigh et al. [24] considers only the circumferential strain estimated from tagged MR images as the mechanical activation measure. Another approach has been developed using a mathematical based computational technique to image the active stress from the displacement using an inverse model [17]. This method was able to reconstruct traveling plane wave of active stress from a mechanical deformation. The active stress was initially used to generate this deformation using a forward model. However, this method would still need to be evaluated in clinical application. Compared to [16], instead of estimating displacements and strains directly from the E/M model, we propose a more realistic estimation by first simulating 3D images and then using an image-based motion tracking algorithm. Furthermore, rather than learning the activation forces over time, we have chosen to learn the depolarization times of all American Heart Association (AHA) segments. Finally, our learning approach is optimized in order to detect which kinematic descriptor is most correlated with the electrophysiology waves.

The overall approach is described in Fig. 1 and mainly

consists in three stages. First, right and left ventricles are segmented from an input cardiac image sequence and the cardiac motion is tracked. An electromechanical model of the heart is mechanically calibrated from this data. In a second stage, a training set, *a.k.a* patient-specific database, is created from this E/M model by changing electrophysiological parameters related to different pathological conditions. For each set of electrophysiology parameters, a different cardiac motion is simulated and a realistic synthetic image sequence is created. In the third stage, motion descriptors are estimated from each sequence. A learning method is then trained to relate those descriptors with the endocardial depolarization times. Finally, the depolarization times of the original sequence are estimated from the knowledge of its motion descriptors. Evaluation of the inverse electro-kinematic learning process on three patients is discussed in Sec. V.

II. Image Processing and Parameter Calibration

A. Image Segmentation and Registration

First we need to apply two image processing steps to the patient clinical image sequence. These steps are the segmentation of the end diastolic (ED) myocardium and the estimation of the myocardium motion. The purpose of the segmentation is to personalize the cardiac mesh geometry required for the cardiac E/M simulation. Furthermore, the estimation of patient cardiac motion allows us to also estimate the patient's endocardial left ventricle (LV) volume curve. Using this information, The E/M simulation can be calibrated with respect to this volume curve so that the simulated ejection fraction as well as the ejection and filling rates are similar to the measured ones [25].

The 3D epicardium and endocardium of the left and the right ventricles of the ED clinical image were delineated using an interactive tool available within the CardioViz3D software [26]. These delineations were then used to create the myocardium segmentation. Using CGAL software [27], a computational tetrahedral mesh was created from the binary mask of the compact myocardium segmentation (cf. Fig. 2). We label the different tetrahedra of the mesh in order to set different electrical conduction parameters for each labeled region (Sec. III-A). The labels include the scar, the Purkinje network (the tetrahedra next to the endocardial surface), the scarred Purkinje network (the intersection of the scar and the Purkinje network) and the cardiac muscle (the remaining tetrahedra). To create bull-eyes plot, we also label the left ventricle according to the 17 AHA segments.

Applying a non-linear registration to pairs of medical images is a common method to estimate the motion of the tissue in the image. Here we use the symmetric log-domain diffeomorphic demons (LogDemons) [28] non-rigid registration method to align the template image $T_i(\mathbf{x})$ to a reference image $R(\mathbf{x})$, which is the ED image of the clinical sequence, by estimating a dense non-linear transformation $\phi_i(\mathbf{x})$, where $\mathbf{x} \in \mathbb{R}^3$ is the space coordinate. $T_i(\mathbf{x})$ is the image at each time frame i in the cardiac sequence. This transformation $\phi_i(\mathbf{x})$ is associated with the displacement vector field $u_i(\mathbf{x})$ and is parameterized by the stationary velocity field $v_i(\mathbf{x})$ which ensures the invertibility of the deformation since we

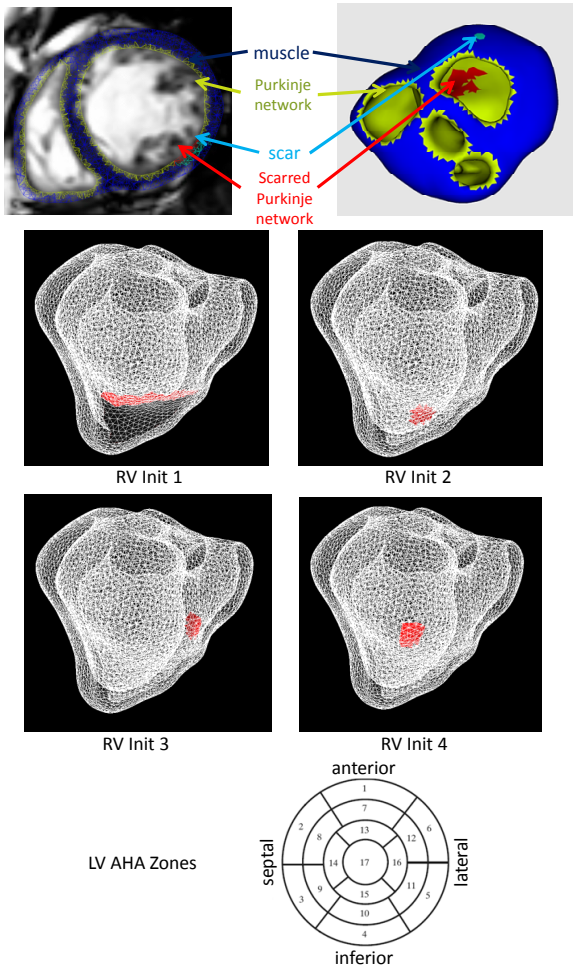

Fig. 2. **Cardiac Geometry and Electrical Stimulation.** A personalized cardiac mesh is created from the myocardium delineation of the clinical image. The region on the surface of the LV and RV endocardium is set to have higher electrical conduction velocity to simulate the Purkinje network. Different RV initial electrical activation position is set to simulate the extremities of the Bundle of His. These positions are approximately set based on the septal LV AHA Zones.

are working in the log-domain. By having this estimated displacement field, we are also able to estimate the patient's endocardial LV volume curve in time. We deformed the ED tetrahedral mesh using the estimated displacement field $u_i(\mathbf{x})$ and then computed the endocardial LV volume of the deformed mesh in time.

B. Electromechanical Model Calibration

We used the Eikonal model to simulate the electrophysiological activation patterns. This model has the advantage to be fast to compute and involves few parameters. More detailed models [29], [30] could also have been used however such additional level of complexity is not necessary since we are only interested in providing main patterns of conduction driven by few parameters. The Eikonal equation $v\sqrt{\nabla T_d^t D \nabla T_d} = 1$ was solved using Multi-Front Fast Marching Method [31] to calculate the depolarization time T_d at each point of the mesh. v is the local conduction velocity and $D = (1-r)f \otimes f + r.I$ is the anisotropic conductivity tensor where f is the fiber

orientation, r is the conductivity anisotropy ratio and I is the identity matrix.

We base our approach on the Bestel-Clément-Sorine (BCS) E/M model [32] composed of a passive non linear elastic part and an active part that describes the binding and unbinding process of the actin and myosin filaments in the sarcomere by a differential equation that controls the active stress τ_c and the sarcomere stiffness k_c:

$$\begin{cases} \dot{k_c} = -(\mid u \mid +\alpha \mid \dot{e_c} \mid)k_c + n_0 k_0 \mid u \mid_+ \\ \dot{\tau_c} = -(\mid u \mid +\alpha \mid \dot{e_c} \mid)\tau_c + \dot{e_c} k_c + n_0 \sigma_0 \mid u \mid_+ \end{cases} \quad (1)$$

where α is a constant related to the cross-bridge release due to a high contraction rate, k_0 and σ_0 are respectively the maximum stiffness and contraction. n_0 is a reduction factor that allows to take into account *the Starling effect* by which the maximum contraction depends on the fiber strain e_c. The control variable u is derived from the electrical activation model and is a function of the free calcium concentration only. It is modeled using electrophysiological inputs such as depolarization times (T_d) and action potential durations (APD). The four-element Windkessel model is used to model the arterial pressure [25].

The BCS E/M model was implemented in the SOFA simulation platform [33] and to assess the mechanical parameters of the model, we used the algorithm derived from the Unscented Transform [34], and described in [25], [35]. The algorithm finds a set of parameters that enable the simulation to match observations on the endocardial LV volume (the minimum volume, the minimum and maximum of the flow) in one iteration through the analysis of the covariance matrix between the simulated observations and the variation of each parameter independently. The assessed calibrated parameters of the BCS E/M model are σ_0, K, μ, APD and Rp. K is the Bulk modulus of the passive part and μ is the viscosity parameter of the active part. APD is the cell excitation duration. Rp is the peripheral resistance, one of the Windkessel parameters.

III. Patient-Specific Database of Synthetic Image Sequences

A database of visually realistic synthetic cardiac sequences is created using the method proposed in [22]. This database is required to train the machine learning algorithm. This synthetic sequence generation method consists in the combination of the simulated motion and the real motion estimated from the patient image sequence. The database is built using different scenarios which are performed to simulate a variety of conditions close to clinical condition of this patient. Since these datasets are taken from patients with a left bundle branch block (LBBB), the scenarios consist of different variations of electrophysiological and mechanical parameters that simulate this specific pathology.

A. Simulated Electromechanical Conditions

An electrophysiological activation pattern which corresponds to each scenario is generated using the Eikonal model in the personalized cardiac mesh geometry. The scenarios are created based on a variation of the parameters of the Eikonal model around the standard values. The varying parameters are the conduction velocity value of the Purkinje network v_p, the value in the cardiac muscle v_m, and also the initial electrical activation position which simulates the extremities of the Bundle of His. For datasets containing a scar region, a variation of the conduction velocity value for this region v_s and also a value of the scarred Purkinje network v_{sp} are also included in the scenarios (cf. Table I and Fig. 2).

Electrical Onset Position	Conduction Velocities in cm/s of: Muscle v_m	Purkinje v_p	Scar v_s	Scarred Purkinje v_{sp}
1-2-3-4	40-50-80-110	160-240-350	5-10-20	120

TABLE I
Patient-Specific Database of 144 Simulated Cases. We varied the initial electrical activation position of the LBBB and the conduction velocities of the different components of the electrophysiological model.

Electrical Onset Position	Conduction Velocities in cm/s of: Muscle v_m	Purkinje v_p	Block v_b	Blocked Purkinje v_{bp}
1-2-3-4	30-50-80	130-210-320	none- 30 (Anterior)- 30 (Posterior)	none- 30-90 (Anterior)- 30-90 (Posterior)

TABLE II
Patient-Specific Database of 180 Simulated Cases. Additional configurations with low conduction velocity in the anterior lateral region or in the inferior lateral region are added to mimic the functional block.

For datasets that do not contain a scar region, we set a low conduction velocity in the anterior lateral region (zone 6, 12, and 16 of the AHA segments) or in the inferior lateral region (zone 5, 11, and 16 of the AHA segments) in order to mimic the occurrence of a functional block in those regions (cf. Table II). The overall conduction velocities are also set lower compared to Table I.

B. Generation of Synthetic Image Sequences

Visually realistic synthetic time series of MR images were created using the previously simulated deformation which was combined to the real clinical sequence estimated displacement using the method proposed in [22]. This method applied non-rigid registration algorithm to extract the motion of the real clinical MRI sequence. This extracted motion was then combined with the E/M simulated motion in the log domain and then used to warp the original images in order to create the synthetic cardiac sequence. With this method, a database of realistic images of the patient was generated for which the underlying cardiac motion and electrophysiological parameters are known. This database served as the training set in our machine learning based study. For each different initial electrical activation position (RV Init 1, 2, 3 and 4) (cf. Fig. 2, Table I and Table II), a mechanical calibration is performed as described in section II-B. Therefore, the variation of the mechanical parameters were included as well in the database.

With the method described previously, a large database of synthetic 3D MR images was created. We then tracked the cardiac motion from those synthetic images by using the symmetric log-domain diffeomorphic demons (LogDemons) registration algorithm [28]. More precisely, we registered all the images of the synthetic sequence to its reference ED image as we did to the real clinical sequence.

IV. Inverse Electro-Kinematic Learning

A. Cardiac Motion Descriptors

As an input to a machine learning algorithm, we needed to first extract kinematic descriptors which describe in a compact and discriminative way the cardiac motion for each time point in the cardiac cycle. We wanted these descriptors to be regional, as we aim for an activation pattern rather than local activation times, and also intrinsic (frame invariant) as the orientation of the heart in the images varies.

To this end, we first characterized the motion of each AHA segment by fitting in the least-squares sense an affine transformation $f(p) = Ap + B$ to the LogDemons estimated displacement field. The strain tensor E was then computed from the affine matrix A as: $E = (A^T A - I)/2$.

We then extracted kinematic descriptors at each time of the cardiac cycle that are invariant to any change of reference frame (or rigid transformation). For the strain matrix E, the three Euclidean invariants are computed as:

$$x_1 = \text{trace}(E),\ x_2 = \text{trace}(E^2),\ x_3 = \det(E)$$

For the displacement vector, we only extracted its norm as invariant:

$$x_4 = \|u\| = \|Ab + B - b\|,$$

where $\|u\|$ is the displacement norm of the zone centroid with b the initial position of the centroid. We also used the strain in the direction of displacement as the invariant:

$$x_5 = (u^T E u)/(2\|u\|^2)$$

Compared to our previous study [15], we added here more descriptors which are usually found in clinical records. We added the QRS duration $x_6 = t_{QRS}$ which is the time needed for the whole myocardium to be activated. We also added the LV volume curve $x_7 = V$ and the regional LV volume curve $x_8 = V_{reg}$ computed for each AHA segment. More precisely, we divided the LV endocardial surface according to the AHA segment surfaces and then computed the volume of the region created by each displaced segment surface and the barycenter of the LV (cf. Fig. 3).

Furthermore, in order to learn the influence of the dynamics of some descriptors, we added the derivative of the trace of the strain tensor, of the displacement, and of the global and regional volume curves:

$$x_9 = d\,\text{trace}(E)/dt,\ x_{10} = d\|u\|/dt,$$

$$x_{11} = dV/dt, x_{12} = dV_{reg}/dt$$

These descriptors, except for the volume curve x_7, its derivative x_{11} and the QRS duration x_6, are evaluated regionally for the 17 AHA zones during the n time instances. The value

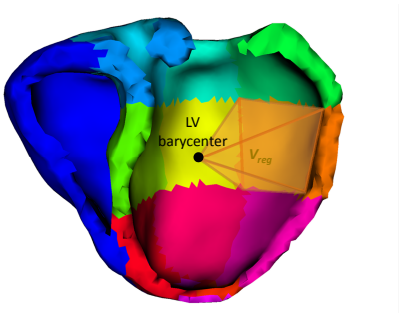

Fig. 3. **Regional LV Volume.** The V_{reg} is the volume of the region created by the LV AHA segment surface and the LV barycenter.

n depends on the temporal resolution of the original clinical sequence, n = number of frames $-$ 1. The volume curve x_7 and its derivative x_{11} are vectors with length of n and the QRS duration x_6 is a single scalar value.

The difficulty in using a simulated database for machine-learning is that there are limitations in both the electromechanical model used to simulate the motion and the image processing methods used to extract the descriptors. Therefore there can be discrepancies between the descriptors used in the learning phase compared to the descriptors extracted from the real images.

In order to cope with this, and also because we are more interested in the relative dynamics of these descriptors which is related to the activation pattern than in their absolute values, we normalized each descriptor. This normalization was done regionally for the descriptors taken from the 17 AHA regions. With this normalization, each descriptor has a range of values from 0 to 1, as we use the relationship $x = (x - x_{min})/(x_{max} - x_{min})$, where x_{max} and x_{min} are the maximum and the minimum values of x respectively. .

Number	Descriptor	Vector Size
x_1	trace(E)	17×n
x_2	trace(E^2)	17×n
x_3	det(E)	17×n
x_4	$\|u\|$	17×n
x_5	$(u^T E u)/(2\|u\|^2)$	17×n
x_6	t_{QRS}	1
x_7	V	n
x_8	V_{reg}	17×n
x_9	dx_1/dt	17×n
x_{10}	dx_4/dt	17×n
x_{11}	dx_7/dt	n
x_{12}	dx_8/dt	17×n

TABLE III
List of the Descriptors. The descriptors are extracted from the estimated cardiac motion, their temporal derivation and also the QRS duration. n = the number of frames in a cardiac cycle - 1.

These 12 descriptors (cf. Table. III) were used to create a kinematic descriptor vector $\mathbf{x} = (x_i)_{i\in[1,12]} \in \mathbb{R}^d$ for each

simulation with

$$\begin{aligned} d &= 9(\text{Descriptors}_{1,2,3,4,5,8,9,10,12}) \times n(\text{Times}) \times 17(\text{Zones}) \\ &+ 2(\text{Descriptors}_{7,11}) \times n(\text{Times}) \\ &+ 1(\text{Descriptors}_{6}) \\ &= 155n + 1 \end{aligned}$$

For a cardiac image sequence with 30 images, the dimension d of the complete vectorial kinematic descriptor is:
$d = 155 \times (30 - 1) + 1 = 4496$.

B. Machine Learning Method

In the inverse electro-kinematic learning process, the non-linear relationship between the kinematic descriptors and the electrical propagation was estimated based on a training set extracted from the synthetic database. To represent the cardiac electrophysiology, we considered the activation time when the electrical potential starts to depolarize at a point of the myocardium. The activation time was averaged for all points of the LV endocardial surface in each AHA segment. Therefore, the vector characterizing electrophysiology for each simulation is $\mathbf{y} = (y_i) \in \mathbb{R}^{\text{r=17 (AHA Zones)}} = log(\text{Activation Times})$.

We modeled the non-linear relationship using Least-Square Support Vector Machine (LS-SVM) for regression [36] which is similar to the Kernel Ridge Regression (KRR).

LS-SVM extends the KRR method by adding a bias term. KRR itself is the non-linear extension of Ridge Regression (RR) which searches a linear function $\mathbf{y} = \mathbf{w}^T\mathbf{x}$ that models the dependencies between the descriptor vectors $\mathbf{x} = \mathbf{x}_i \in \mathbb{R}^d$ and response vectors $\mathbf{y} = \mathrm{y}_i \in \mathbb{R}^r$ (all vectors are column vectors) from a set of N examples $(\mathrm{x}_1, \mathrm{y}_1), (\mathrm{x}_2, \mathrm{y}_2), ..., (\mathrm{x}_N, \mathrm{y}_N)$. The use of nonlinear kernels allows to capture the complex relationship between activation times and motion in a way that will decrease the influence of some descriptors when far from the ones used in the training phase.
Ridge Regression can be extended to Kernel Ridge Regression by rewriting the solution

$$\begin{aligned} \mathrm{y} &= \mathrm{w}^T\mathrm{x} \\ &= Y^T(\lambda\mathrm{I} + K)^{-1}\mathrm{k} \end{aligned} \tag{2}$$

with $K = XX^T$, $\mathrm{k} = X\mathrm{x}$, $\lambda > 0$ is the regularization parameter, $X = (\mathrm{x}_1, \mathrm{x}_2, ..., \mathrm{x}_N)^T$ is a $N \times d$ matrix and $Y = (\mathrm{y}_1, \mathrm{y}_2, ..., \mathrm{y}_N)^T$ is a $N \times r$ matrix. In this form, other type of Kernel function can be used to substitute the linear Kernel function $K = K(\mathrm{x}_i, \mathrm{x}_j) = \mathrm{x}_i^T\mathrm{x}_j$.

We modelled the non-linear relationship using Kernel Ridge Regression with a bias term or Least-Square Support Vector Machine (LS-SVM) for regression

$$\mathrm{y} = f(\mathrm{x}) = A\mathrm{k}(\mathrm{x}_i, \mathrm{x}) + \mathrm{b} \tag{3}$$

with matrix A is computed as $A = Y^T(\lambda\mathrm{I} + K)^{-1}$ and $\mathrm{k}(\mathrm{x}_i, \mathrm{x})$ is a kernel vector. We chose the Radial Basis Function (RBF) $K(\mathrm{x}_i, \mathrm{x}_j) = \sum_{k=1}^{D} e^{-z_k}$ as the Kernel function where $z_k = \left(\left|\mathrm{x}_i^k - \mathrm{x}_j^k\right| / (\sigma_k\alpha_k)\right)^2$, $i, j = \{1, ..., N\}$ and D is the number of descriptors. In this kernel function, σ_k is the standard deviation of each descriptor and α_k is a dimensionless coefficient which weights the importance of each descriptor in the learning process, where $\sigma_k^2 = (1/N)\sum_{i=1}^{N}\left\|\mathrm{x}_i^k - \mu\right\|^2$ and $\mu = (1/N)\sum_{i=1}^{N}\mathrm{x}_i^k$.

C. Parameter Optimization

The chosen λ and α parameters are optimized by using leave-one-out estimates which train the model with all members of the training set but one and test the performance on the singleton. The process is repeated for all the singletons in the training set. We use Allen's PRESS (Predicted Residual Sum of Squares) criterion for the optimization of the λ and α parameters $PRESS = \sum_i^N \mathrm{e}_{(i)}^2$ [36] where $\mathrm{e}_{(i)} = \mathrm{y}_i - \hat{\mathrm{y}}_{(i)}$ is the residual for the *i*th example with the *i*th example excluded from the training process and $\hat{\mathrm{y}}_{(i)}$ is the predicted response for the *i*th example based on the training process. Fortunately, we have $e_{(i)} = e_i/(1 - h_{ii})$ where $e_i = \mathrm{y}_i - \hat{\mathrm{y}}_i$ is the residual for the *i*th example in the training process which includes all examples and $\hat{\mathrm{y}}_i$ is fitted response based on this training. h_{ii} is the *i*th element of the leading diagonal of the hat matrix $H = X(\lambda\mathrm{I} + X^TX)^{-1}X^T = XX^T(\lambda\mathrm{I} + XX^T = K(\lambda\mathrm{I} + K)^{-1}$. Therefore, in the end, we can have the PRESS for the chosen parameters λ and α in one iteration without having to do N iterations for the leave-one-out cross validation. We use the Powell's BOBYQA [37], [38] method to optimize these parameters to have the smallest PRESS.

V. Results

A. Activation Pattern Validation on Synthetic Data

First, we evaluated the learning process on the generated synthetic data and estimated the minimum size of the training set to have a small regression error for the remaining entries of the database. Fig. 4 shows a good generalization with a root mean square (RMS) error of less than 8 ms of residual by using at least 13, 18 and 44 training datasets for the Database I, II and III respectively. The Database I, II, and III are the patient-specific databases for patient I, II and III respectively described in Sec. V-B. These numbers are less than 25% of the size of datasets of each database.

B. Activation Pattern Evaluation on Clinical Data

We applied our proposed approach on three clinical cases from patients with different pathologies and etiologies or causes of diseases. However, in all three of them there was a modified activation pattern due to scars or functional blocks, as well as poor ejection fraction, which are the characteristics of the patient groups we are aiming at.

The first patient was a 60 years old woman with heart failure and NYHA class III symptoms. She had subendocardial postero-lateral scar in the left ventricle. Her left ventricular ejection fraction was 25% on maximal tolerated heart failure medication. The surface ECG demonstrated significant conduction disease with left bundle branch block (LBBB) QRS duration of 154 ms (normal QRS is less than 120 ms). Echocardiography, including Tissue Doppler, confirmed significant mechanical dysynchrony in keeping with the ECG findings.

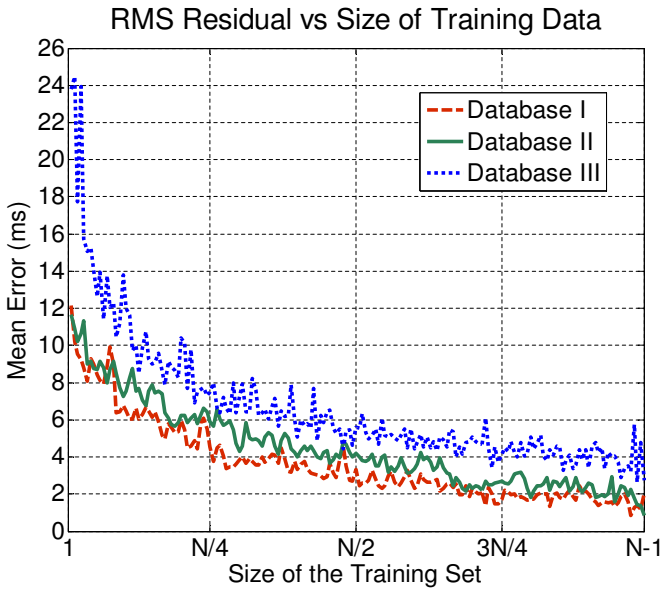

Fig. 4. **RMS Residual vs Size of Training Data.** Less than 8 ms RMS residual is obtained by using more than 13, 18 and 44 training cases for the Database I, II and III respectively. The Database I, II, and III are the patient-specific databases for patient I, II and III respectively described in Sec. V-B. This means that a good generalization is obtained by using less than 25% of the whole dataset.

The second patient was a 72 years old male patient with ischemic heart disease. He had a myocardial infarction in the infero-lateral wall. His left ventricular ejection fraction was 35% with the QRS duration of 99 ms.

The third patient was a seventy-seven year old woman with a much more developed dilated cardiomyopathy. She was in NYHA class III heart failure with a LV ejection fraction of 18% and LBBB QRS duration of 200 ms. There was no late gadolinium enhancement images acquired but functional conduction block was observed in the electrophysiological mapping. We proposed to add different virtual functional blocks in the simulated database in order to be able to correctly estimate the activation patterns in non ischemic cases, which often also present conduction blocks.

For all the cases, dynamic cardiac MRI (Philips 1.5T Achieva, Phillips Healthcare, Best, The Netherlands) consisted of multiple slice cine steady state free precession (SSFP) scans performed in short-axis orientation to assess the ventricular function (TR/TE = 2.9/1.5ms, resolution $2.2 \times 2.2 \times 10\ mm^3$, around 30 heart phases, breath-hold). The images were then resampled in a resolution of 1.6 mm^3 and centered on the heart region with a region of interest of around 100^3 voxels. A non-contact mapping study was performed using the Ensite 3000 multi-electrode array catheter system (St Jude, Sylmar, CA). The array records intracavity far-field potentials that are sampled at 1.2 kHz and digitally filtered at 0.1-300 Hz. The resulting signals allow the reconstruction of over 3000 virtual unipolar electrograms superimposed on a model of the left ventricle created using a locator signal on a roving endocardial catheter. The XMR fusion provided the location of the Ensite mapping with respect to the MR-derived information.

For each patient, a database of synthetic sequences which contains the scenarios described in Sec. III-A was built. For the first patient, the total generated synthetic 3D MR images are 144 (scenarios) $\times$ 29 (number of frame - 1) = 4176.

We did a first evaluation of this learning process on the clinical 3D MR sequence of the patients. Using the relationship or the optimized parameters previously found, we are able to predict the LV endocardial electrical activation time of the patient. We apply the same processing to this sequence as we did for the synthetic sequence.

After optimizing the PRESS criterion on the whole synthetic database of each patient, the obtained LS-SVM parameters are shown in Table. IV. We listed the descriptors with their $(\alpha_{max} - \alpha_i)/(\alpha_{max} - \alpha_{min})$ value which describes the increasing importance of the descriptor i (cf. Table. IV). α_{max} and α_{min} are respectively the maximum and minimum α value of the descriptors for a patient database. Therefore the value range is from 0 for the least important descriptor to 1 for the most important one. Table. IV shows that the kinematic descriptors $x_1 = \text{trace}(E)$ and $x_5 = (u^T E u)/(2\|u\|^2)$ are consistently the most important ones to learn the electro-kinematic relationship from the three databases since they have smaller optimized α_i values compared to the other descriptors.

Descriptor	$(\alpha_{max}-\alpha_i)/(\alpha_{max}-\alpha_{min})$		
	Patient I	Patient II	Patient III
trace(E)	1.000	0.522	0.514
trace(E^2)	0.541	0.431	0.446
det(E)	0.506	0.000	0.464
$\|u\|$	0.428	0.823	1.000
$(u^T E u)/(2\|u\|^2)$	0.659	1.000	0.998
t_{QRS}	0.000	0.167	0.040
V	0.046	0.227	0.097
V_{reg}	0.103	0.203	0.053
d trace(E) / dt	0.367	0.189	0.171
$d\ \|u\| / dt$	0.597	0.282	0.078
$d\ V / dt$	0.239	0.520	0.232
$d\ V_{reg} / dt$	0.218	0.279	0.000
α_{min}	1.038	1.690	0.985
α_{max}	2.263	2.282	2.583

TABLE IV
RANK OF THE OPTIMIZED LS-SVM PARAMETERS. THE VALUE OF THE PARAMETERS $(\alpha_{max} - \alpha_i)/(\alpha_{max} - \alpha_{min})$ AFTER OPTIMIZING THE PRESS CRITERION GIVES THE IMPORTANCE OF EACH DESCRIPTOR.

After performing LogDemons non-rigid registration and extracting the vector $\mathbf{x}$ of kinematic descriptors from the estimated displacement field, the electrophysiology vector $\mathbf{y}$ was estimated from the LS-SVM. Since we have the ground truth LV endocardial electrical activation time of the patient acquired using non-contact mapping study, we are able to compare our prediction with this measurement. Similar estimated depolarization times were obtained for this patient (cf. Fig. 5) with the root mean square error RMSE = 11.20 ms for the

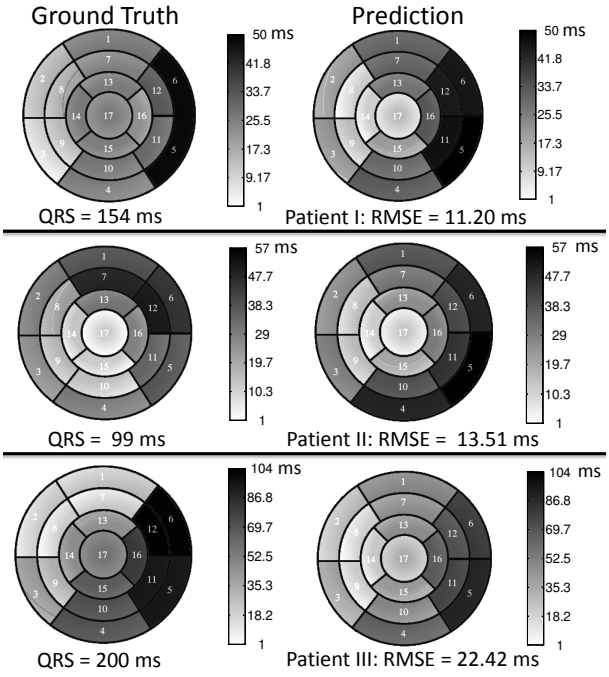

Fig. 5. **Depolarization Time Estimation from Clinical 3D MR Sequences.** First evaluation of the learning process in the prediction of the LV endocardial surface depolarization time on three patients (right) is compared to the ground truth value (left). Similar patterns in the same range are observed on the three of them.

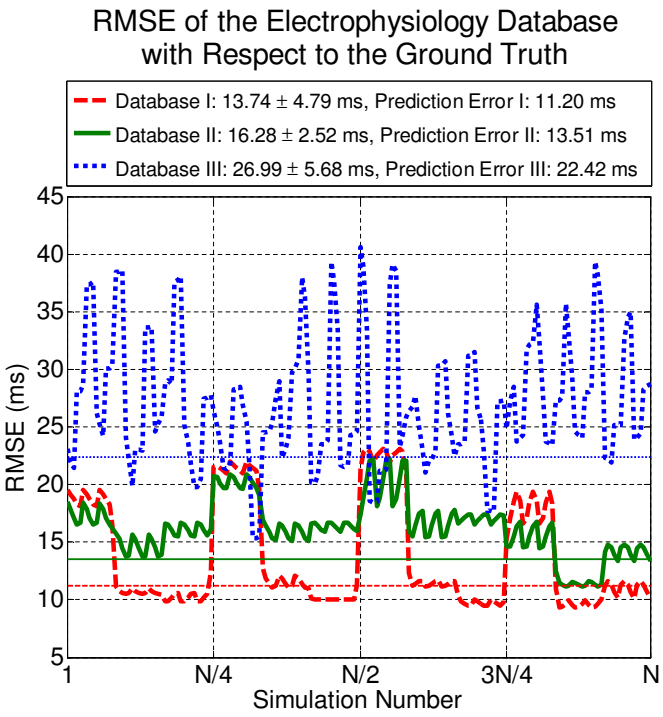

Fig. 6. **Distance (RMSE) of Each Simulated Electrophysiology with respect to the Patient's Ground Truth.** For each patient's database of simulated electrophysiological patterns, the difference of each pattern with the patient's electrophysiological pattern ground truth is calculated. These differences are shown in a curve which describes the variation of the simulated electrophysiology. The mean and standard deviation of each curve for each patient are shown in the legend. The prediction errors in Fig. 5 are shown as horizontal lines with the values shown in the legend.

patient I, 13.51 ms for the patient II and 22.42 ms for the patient III.

We computed the mean and variance of the electrophysiological database created previously with the patient's LV endocardial electrical activation time ground truth value. Then, we were able to compare our prediction with these values (cf. Fig. 6).

We can observe similar RMS errors for the activation time for different parameter sets, which is mostly due to the influence of the Purkinje network. The high electrical conductivity of the Purkinje network produces similar endocardial activation patterns. However, the activation pattern for the whole myocardium is significantly different for each parameter set, which makes the resulting motion pattern different.

VI. Discussion

In this study, we created patient-specific database of synthetic sequences in order to learn the cardiac inverse electro-kinematic relationship. In the end, we used the learned relationship to estimate patient's left ventricle endocardium electrical activation time. For each dataset, the prediction error (cf. Fig. 5) is in the order of 15 ms which represents typically between 21% and 24% of the total LV endocardium surface activation and between 7% and 14% of the QRS duration. This is reasonable given the spatial and temporal accuracy of the invasive intra-cardiac mapping systems and even more compared to the accuracy of non-invasive ECGI systems.

A current limitation of the method is the spatial resolution of the predicted map. The spatial resolution of the estimated activation pattern could be increased to more than 17 regions as the electromechanical model spatial resolution is much finer. However given the resolution of the images and the uncertainty on the invasive EP data (due to acquisition and registration errors), predicting depolarization times at a greater spatial resolution would be difficult to validate with the current data. However, the modelling and the learning phases can handle higher resolution data therefore the method would be unchanged. We are working on acquiring higher resolution contact maps to allow us to have a better validation for a finer model.

The prediction error is also smaller compared to the average error in the database (cf. Fig. 6). Patient I: 11.20 ms $<$ 13.74 ms, Patient II: 13.51 ms $<$ 16.28 ms, Patient III: 22.42 ms $<$ 26.99 ms. This shows the proper behavior of the LS-SVM method since it basically consists in interpolating the depolarization times of the entries in the learning set that are closest to the input kinematics descriptors. Ideally, a measure of confidence in the prediction should be provided, but the LS-SVM regression method does not provide any covariance on the activation times. Covariance can only be estimated on the activation parameters if covariance on the motion descriptors is available which is not the case here.

With this learning process, the prediction error combines several types of possible errors: noise in the non-contact mapping acquisition, errors in the learning process, errors in modeling the cardiac electromechanics and discretization

errors. Due to the non-contact nature of the mapping, it is often difficult to have an accurate match between the electrophysiology maps and the endocardial surface reconstructed from MR imaging. For example for Patient II, there is an uncertainty in the ground truth data since the latest activated area is not in the region where the scar is. Applying 30° of clockwise rotation to the ground truth data would make the scarred region last activated and reduce the prediction error from 13.51 ms to 8.73 ms. The learning error mostly depends on the size of the electrophysiology scenarios as they should be vast enough to include the actual pathology of the patient. In this paper, we have restricted ourselves to LBBB cases with 5 parameter categories (onset position, conduction velocity...) leading to between 144 and 180 simulated cases. Adding more hypothesis of electrophysiology parameters in the training set would help capturing more complex electrophysiology and kinematics patterns. However, this would also lead to a much increased number of simulations and therefore a trade-off must be found between the range of pathologies and the computational requirements.

Then prediction errors also depend on the accuracy of the electrophysiology model. For instance, applying an automated personalization method [39] of an electrophysiology model on the 3 patients' datasets described previously leads to errors of 10.19 ms, 9.19 ms and 16.51 ms respectively. These errors after personalization capture the combined effect of acquisition, discretization and model errors. Given that the prediction errors are respectively 11.20 ms, 13.51 ms and 22.42 ms, it appears that the errors due to the learning process are relatively small. To decrease further those errors may require to use a more complex electrophysiological model or a finer mesh. However, it is probable that improving the acquisition protocol leading to higher spatial resolution would be most beneficial. In practice, obtaining ground truth electrophysiology data is currently difficult due to the invasive nature of the endocardial mapping systems. Using less invasive electrophysiology data from body surface potential mapping would allow to broaden the number of test cases.

In addition, to decrease the prediction errors, it is important that the electromechanical model produces realistic simulations of the cardiac motion. This not only implies that the cardiac physiology is well described by the chosen E/M model, but it also means that this model is sufficiently well personalized. In our approach, the chosen E/M has been shown to produce realistic simulations of the cardiac motion and also shown good predictive behavior for the electrophysiology and mechanics [40]. Furthermore, in this study, we have performed four different mechanical calibrations for each onset position, in order to have similar volume curves between the simulation and the patient data. To improve the prediction, one would probably need to perform a calibration and even a personalization of the mechanical parameters for each electrophysiology scenario. Indeed, the calibration stage only tries to match the endocardial volume curves whereas the personalization stage tries to match more regional or local kinematic indices (regional volume curves, estimated displacement...). The weighting of the descriptors was learned on the simulated database, therefore it is important that the link between electromechanics and deformation is well captured by the model. Any improvement of the model can be readily used in this method by re-running the learning phase.
The learning phase will be also influenced by the observability of the deformation features in the motion extracted from the simulated images. Any improvement in cardiac motion tracking from images would help in better learning the link between the simulations and the resulting features. More sophisticated methods for cardiac motion analysis, e.g. atlas-based ones, could be used as input to the learning process, however they still need a large scale validation therefore we focused here on motion descriptors already available in a clinical setting.

One limitation of this study is that the created database is patient-specific. Therefore, numerous simulations need to be performed in order to predict another patient's depolarization time. Currently, predictions from one training set built from one patient does not generalize to another patient because of the difference in their kinematic descriptors. The use of an atlas may overcome this limitation but meaningful strategies to transport the kinematic descriptors between patients have to be found.

VII. Conclusion

As the generated synthetic cardiac MR sequences have electro-kinematic "ground truth" information, we have performed an inverse electro-kinematic learning on this patient-specific database. Invariant kinematic descriptors were extracted from the displacement field obtained from the sequence registration. The non-linear inverse relationship between the electrical activation times and the kinematic descriptors was modeled using LS-SVM. Evaluation of the learning process for the database of synthetic sequence shows good generalization and a first evaluation on three clinical MR sequences shows encouraging results.

We presented here results on patients with a LBBB in order to reduce the span of possible onset locations and have a relatively slower propagation (large QRS). However we tested the method on both ischemic and non-ischemic patients. The results are better for the ischemic patients, as the scar locations are known, while for the non-ischemic patients we need to find where the potential functional block is. Extension of this method to more complex activation patterns should be possible, but the evaluation of the observability of such patterns from the available time resolution of the images has to be explored.

This approach opens the possibility of using non-invasive cardiac motion imaging as a way to estimate electrophysiological patterns. This could provide additional information to the cardiologist during the optimization of the Cardiac Resynchronization Therapy (CRT), for example allowing the placement of the pacemaker leads in the cardiac region which is lately activated. An extension of this work would be the application of this method to different imaging modalities. This can be done since the synthetic sequence generation method is generic and was already demonstrated for different imaging modalities [22].

ACKNOWLEDGMENTS

The authors acknowledge the support of the MedYMA advanced grant 291080 funded by the European Research Council (ERC). The authors warmly thank Stéphanie Marchesseau and Jatin Relan from the Asclepios team, Pascal Cathier and Patrick Etyngier from the Medysis Research Lab and Eric Saloux from the Caen University Hospital for the fruitful discussion.

REFERENCES

[1] R. N. Ghanem, P. Jia, C. Ramanathan, K. Ryu, A. Markowitz, and Y. Rudy, "Noninvasive electrocardiographic imaging (ECGI): comparison to intraoperative mapping in patients," *Heart Rhythm*, vol. 2, pp. 339–354, Apr 2005.

[2] C. Ramanathan, R. N. Ghanem, P. Jia, K. Ryu, and Y. Rudy, "Noninvasive electrocardiographic imaging for cardiac electrophysiology and arrhythmia." *Nature Medicine*, vol. 10, no. 4, pp. 422–8, 2004.

[3] Y. Wang, P. Cuculich, J. Zhang, K. Desouza, R. Vijayakumar, J. Chen, M. Faddis, B. Lindsay, T. Smith, and Y. Rudy, "Noninvasive electroanatomic mapping of human ventricular arrhythmias with electrocardiographic imaging." *Science Translational Medicine*, vol. 3, no. 98, p. 98ra84, 2011.

[4] C. Han, S. M. Pogwizd, C. R. Killingsworth, and B. He, "Noninvasive imaging of three-dimensional cardiac activation sequence during pacing and ventricular tachycardia." *Heart Rhythm*, vol. 8, no. 8, pp. 1266–72, 2011.

[5] ——, "Noninvasive reconstruction of the three-dimensional ventricular activation sequence during pacing and ventricular tachycardia in the canine heart." *American Journal of Physiology Heart and Circulatory Physiology*, vol. 302, no. 1, pp. H244–52, 2012.

[6] C. Liu, N. Skadsberg, S. Ahlberg, C. Swingen, P. Iaizzo, and B. He, "Estimation of global ventricular activation sequences by noninvasive three-dimensional electrical imaging: validation studies in a swine model during pacing." *Journal of Cardiovascular Electrophysiolgy*, vol. 19, no. 5, pp. 535–40, 2008.

[7] X. Zhang, I. Ramachandra, Z. Liu, B. Muneer, S. M. Pogwizd, and B. He, "Noninvasive three-dimensional electrocardiographic imaging of ventricular activation sequence." *American Journal of Physiology Heart and Circulatory Physiology*, vol. 289, no. 6, pp. H2724–H2732, Dec. 2005.

[8] T. Berger, G. Fischer, B. Pfeifer, R. Modre, F. Hanser, T. Trieb, F. Roithinger, M. Stuehlinger, O. Pachinger, B. Tilg, and F. Hintringer, "Single-beat noninvasive imaging of cardiac electrophysiology of ventricular pre-excitation." *Journal of the American College of Cardiology*, vol. 48, no. 10, pp. 2045–52, 2006.

[9] R. H. Helm, M. Byrne, P. A. Helm, S. K. Daya, N. F. Osman, R. Tunin, H. R. Halperin, R. D. Berger, D. A. Kass, and A. C. Lardo, "Three-dimensional mapping of optimal left ventricular pacing site for cardiac resynchronization," *Circulation*, vol. 115, pp. 953–961, February 2007.

[10] M. Sohal, A. Shetty, S. Duckett, Z. Chen, E. Sammut, S. Amraoui, G. Carr-White, R. Razavi, and C. A. Rinaldi, "Non-invasive assessment of left ventricular contraction patterns using cardiac magnetic resonance imaging to identify responders to cardiac resynchronization therapy," *Journal of the American College of Cardiology: Cardiovascular Imaging*, 2013, in press, available online.

[11] K. McLeod, A. Prakosa, T. Mansi, M. Sermesant, and X. Pennec, "An incompressible log-domain demons algorithm for tracking heart tissue," in *Statistical Atlases and Computational Models of the Heart: Imaging and Modelling Challenges*, ser. LNCS, O. Camara, E. Konukoglu, M. Pop, K. Rhode, M. Sermesant, and A. Young, Eds., no. 7085. Toronto, Canada: Springer, Heidelberg, September 2012, pp. 55–67.

[12] C. Tobon-Gomez, M. D. Craene, A. Dahl, S. Kapetanakis, G. Carr-White, A. Lutz, V. Rasche, P. Etyngier, S. Kozerke, T. Schaeffter, C. Riccobene, Y. Martelli, O. Camara, A. F. Frangi, and K. S. Rhode, "A multimodal database for the 1 st cardiac motion analysis challenge," in *Statistical Atlases and Computational Models of the Heart: Imaging and Modelling Challenges*, ser. LNCS, O. Camara, E. Konukoglu, M. Pop, K. Rhode, M. Sermesant, and A. Young, Eds., vol. 7085. Toronto, Canada: Springer, Heidelberg, 2012, pp. 33–44.

[13] T. Mansi, X. Pennec, M. Sermesant, H. Delingette, and N. Ayache, "iLogDemons: A demons-based registration algorithm for tracking incompressible elastic biological tissues," *International Journal of Computer Vision*, vol. 92, pp. 92–111, 2011.

[14] A. Elen, H. F. Choi, D. Loeckx, H. Gao, P. Claus, P. Suetens, F. Maes, and J. D'hooge, "Three-dimensional cardiac strain estimation using spatio-temporal elastic registration of ultrasound images: A feasibility study," *Medical Imaging, IEEE Transactions on*, vol. 27, pp. 1580–1591, 2008.

[15] A. Prakosa, M. Sermesant, H. Delingette, E. Saloux, P. Allain, P. Cathier, P. Etyngier, N. Villain, and N. Ayache, "Synthetic echocardiographic image sequences for cardiac inverse electro-kinematic learning," in *Medical Image Computing and Computer-Assisted Intervention - MICCAI 2011*, ser. LNCS, G. Fichtinger, A. Martel, and T. Peters, Eds., vol. 6891. Toronto, Canada: Springer, Heidelberg, September 2011, pp. 500–507.

[16] ——, "Non-invasive activation times estimation using 3D echocardiography," in *Statistical Atlases and Computational Models of the Heart*, ser. LNCS, O. Camara, M. Pop, K. Rhode, M. Sermesant, N. Smith, and A. Young, Eds., vol. 6364. Beijing, China: Springer, Heidelberg, 2010, pp. 212–221.

[17] N. Otani, S. Luther, R. Singh, and R. Gilmour, "Transmural ultrasound-based visualization of patterns of action potential wave propagation in cardiac tissue," *Annals of Biomedical Engineering*, vol. 38, pp. 3112–3123, 2010.

[18] J. Provost, W. Lee, K. Fujikura, and E. Konofagou, "Electromechanical wave imaging of normal and ischemic hearts in vivo," *Medical Imaging, IEEE Transactions on*, vol. 29, pp. 625–635, March 2010.

[19] G. Sanchez-Ortiz, M. Sermesant, R. Chandrashekara, K. Rhode, R. Razavi, D. Hill, and D. Rueckert, "Detecting the onset of myocardial contraction for establishing inverse electro-mechanical coupling in XMR guided RF ablation," in *Proceedings of International Symposium on Biomedical Imaging*. Arlington: IEEE, 2004, pp. 1055–1058.

[20] E. E. Konofagou and J. Provost, "Electromechanical wave imaging for noninvasive mapping of the 3D electrical activation sequence in canines and humans in vivo," *Journal of Biomechanics*, vol. 45, no. 5, pp. 856 – 864, 2012, special Issue on Cardiovascular Solid Mechanics.

[21] J. Provost, V. Gurev, N. Trayanova, and E. E. Konofagou, "Mapping of cardiac electrical activation with electromechanical wave imaging: An in silicoin vivo reciprocity study," *Heart Rhythm*, vol. 8, no. 5, pp. 752 – 759, 2011.

[22] A. Prakosa, M. Sermesant, H. Delingette, S. Marchesseau, E. Saloux, P. Allain, N. Villain, and N. Ayache, "Generation of synthetic but visually realistic time series of cardiac images combining a biophysical model and clinical images," *Medical Imaging, IEEE Transactions on*, vol. 32, no. 1, pp. 99–109, 2013.

[23] C. Tobon-Gomez, C. Butakoff, S. Aguade, F. Sukno, G. Moragas, and A. Frangi, "Automatic construction of 3D-ASM intensity models by simulating image acquisition: Application to myocardial gated SPECT studies," *Medical Imaging, IEEE Transactions on*, vol. 27, no. 11, pp. 1655 –1667, November 2008.

[24] E. R. McVeigh, F. W. Prinzen, B. T. Wyman, J. E. Tsitlik, H. R. Halperin, and W. C. Hunter, "Imaging asynchronous mechanical activation of the paced heart with tagged MRI," *Magnetic Resonance in Medicine*, vol. 39, pp. 507–513, April 1998.

[25] S. Marchesseau, H. Delingette, M. Sermesant, and N. Ayache, "Fast parameter calibration of a cardiac electromechanical model from medical images based on the unscented transform," *Biomechanics and Modeling in Mechanobiology*, 2012.

[26] N. Toussaint, T. Mansi, H. Delingette, N. Ayache, and M. Sermesant, "An integrated platform for dynamic cardiac simulation and image processing: Application to personalised tetralogy of fallot simulation," in *Proc. Eurographics Workshop on Visual Computing for Biomedicine (VCBM)*, Delft, The Netherlands, 2008.

[27] L. Rineau, S. Tayeb, and M. Yvinec, "3D mesh generation," in *CGAL User and Reference Manual*, 3rd ed., CGAL Editorial Board, Ed., 2009.

[28] T. Vercauteren, X. Pennec, A. Perchant, and N. Ayache, "Symmetric log-domain diffeomorphic registration: A demons-based approach," in *Medical Image Computing and Computer-Assisted Intervention - MICCAI 2008*, ser. LNCS, D. Metaxas, L. Axel, G. Fichtinger, and G. Székely, Eds., vol. 5241. New York, USA: Springer, Heidelberg, September 2008, pp. 754–761.

[29] K. Ten Tusscher, D. Noble, P. Noble, and A. Panfilov, "A model for human ventricular tissue." *American Journal of Physiology*, vol. 286, pp. H1573–H1589, 2004.

[30] C. C. Mitchell and D. G. Schaeffer, "A two current model for the dynamics of cardiac membrane," *Bulletin of Mathematical Biology*, vol. 65, no. 5, pp. 767–793, 2003.

[31] M. Sermesant, E. Konukoglu, H. Delingette, Y. Coudiere, P. Chinchaptanam, K. Rhode, R. Razavi, and N. Ayache, "An anisotropic multi-front fast marching method for real-time simulation of cardiac electrophysiology," in *Proceedings of Functional Imaging and Modeling*

of the Heart 2007 (FIMH'07), ser. LNCS, vol. 4466, 7-9 June 2007, pp. 160–169.

[32] D. Chapelle, P. Le Tallec, P. Moireau, and M. Sorine, "An energy-preserving muscle tissue model: formulation and compatible discretizations," *International Journal for Multiscale Computational Engineering*, vol. 10, no. 2, pp. 189–211, 2012.

[33] F. Faure, C. Duriez, H. Delingette, J. Allard, B. Gilles, S. Marchesseau, H. Talbot, H. Courtecuisse, G. Bousquet, I. Peterlik, and S. Cotin, "Sofa: A multi-model framework for interactive physical simulation," in *Soft Tissue Biomechanical Modeling for Computer Assisted Surgery*, ser. Studies in Mechanobiology, Tissue Engineering and Biomaterials, Y. Payan, Ed. Springer Heidelberg, 2012, vol. 11, pp. 283–321.

[34] S. Julier and J. Uhlmann, "A new extension of the Kalman filter to nonlinear systems," in *International Symposium on Aerospace/Defense Sensing, Simulation and Controls*, vol. 3, 1997, p. 26.

[35] S. Marchesseau, H. Delingette, M. Sermesant, K. Rhode, S. Duckett, C. Rinaldi, R. Razavi, and N. Ayache, "Cardiac mechanical parameter calibration based on the unscented transform," in *Medical Image Computing and Computer-Assisted Intervention - MICCAI 2012*, ser. LNCS, N. Ayache, H. Delingette, P. Golland, and K. Mori, Eds., vol. 7511. Springer, Heidelberg, October 2012, pp. 41–48.

[36] G. C. Cawley, "Leave-one-out cross-validation based model selection criteria for weighted LS-SVMs," in *IJCNN'06*. Vancouver: IEEE, 2006, pp. 1661–1668.

[37] M. J. D. Powell, "The BOBYQA algorithm for bound constrained optimization without derivatives," *DAMTP 2009/NA06*, August 2009.

[38] S. G. Johnson. (2012) The NLopt nonlinear-optimization package. [Online]. Available: http://ab-initio.mit.edu/nlopt

[39] J. Relan, M. Pop, H. Delingette, G. Wright, N. Ayache, and M. Sermesant, "Personalisation of a cardiac electrophysiology model using optical mapping and mri for prediction of changes with pacing," *Bio-Medical Engineering, IEEE Transactions on*, vol. 58, no. 12, pp. 3339–3349, 2011.

[40] M. Sermesant, R. Chabiniok, P. Chinchapatnam, T. Mansi, F. Billet, P. Moireau, J. Peyrat, K. Wong, J. Relan, K. Rhode, M. Ginks, P. Lambiase, H. Delingette, M. Sorine, C. Rinaldi, D. Chapelle, R. Razavi, and N. Ayache, "Patient-specific electromechanical models of the heart for the prediction of pacing acute effects in CRT: A preliminary clinical validation," *Medical Image Analysis*, vol. 16, no. 1, pp. 201–215, 2012.